Centella asiatica Tissue Culture-Derived Extracellular Vesicles: A Multifaceted Approach to Skincare Applications

Tsong-Min Chang[1], Chung-Chin Wu[2], Huey-Chun Huang[3], Shr-Shiuan Wang[1], Ching-Hua Chuang[2], Pei-Lun Kao[2], Wei-Hsuan Tang[2], Luke Tzu-Chi Liu[2], Wei-Yin Qiu[4], Ivona Percec[5], Charles Chen[2, 6], Tsun-Yung Kuo[2*]

[1]Department of Applied Cosmetology, HungKuang University, Taichung City, Taiwan.

[2]Schweitzer Biotech Company, Taipei City, Taiwan

[3]Department of Medical Laboratory Science and Biotechnology, China Medical University, Taichung City, Taiwan

[4]Department of Clinical Application, Center for iPS Cell Research and Application (CiRA), Kyoto University, Kyoto, Japan

[5]Division of Plastic Surgery, Department of Surgery, University of Pennsylvania, Philadelphia, PA, USA

[6]College of Science and Technology, Temple University, Philadelphia, PA, USA

[*]Corresponding author: kingk66.tw@gmail.com

Abstract

Background: *Centella asiatica* has long been used as a medicinal herb in traditional Asian medicine. Its wound healing, skin improvement, and neuroprotective properties have been widely studied. Extracellular vesicles (EVs) are secreted by cells and contain bioactive components with therapeutic properties.

Objectives: This study aims to characterize EVs isolated from *C. asiatica* tissue culture and investigate their therapeutic properties using *in-vitro* assays and UVB-induced damage mouse model.

Methods: EVs were isolated from *C. asiatica* tissue culture and characterized by nanoparticle tracking analysis (NTA) and scanning electron microscopy (SEM). Cytotoxicity, anti-oxidation, anti-melanin, and anti-inflammation of the EVs were evaluated by MTT assay, tyrosinase assay and RT-qPCR in chemical or *in vitro* assays. A UVB-induced photodamage mouse model was established to assess the anti-inflammation effect of EVs *in vivo*. Gels with or without EVs were applied to the damage site and skin appearance was observed daily and skin histopathology was analyzed on day 7 by H&E and immunohistochemical staining.

Results: *C. asiatica* EVs were found to contain high levels of polyphenol and mitigated hydrogen peroxide-induced intracellular ROS. The EVs were further able to reduce intracellular melanin content and tyrosinase activity, and exhibited anti-inflammatory effects by downregulating expression of pro-inflammatory genes COX2 as well as nitric oxide production. In mice with UVB-induced skin damage, daily application of *C. asiatica* EV gel reduced skin epidermis thickness and inflammation compared to UVB-only or blank gel at seven days after UV irradiation.

Conclusions: The beneficial effects of *C. asiatica* EVs on skin quality warrant further studies as promising agents in skin care applications.

Keywords: *Centella asiatica*, skin care, extracellular vesicles, antioxidants, cosmetics,

anti-inflammatory, skin whitening, UV damage, photoaging

Introduction

Centella asiatica, also commonly known as Gotu Kola, is a traditional medicinal herb widely used across Asia [1]. Its broad spectrum of therapeutic properties is attributed to a diverse phytochemical profile, including triterpenoids, flavonoids, and polyphenols, which contribute to the plant's anti-inflammatory, antioxidant, and wound-healing properties, as well as its neuroprotective and cognitive-enhancing effects in animal studies [2-4]. Several key triterpenes, including madecassoside, madecassic acid, asiaticoside, and asiatic acid, are well-studied compounds that play primary roles in the above therapeutic effects [4, 5]. Due to its wide-ranging therapeutic benefits, *C. asiatica* has garnered interest in modern pharmacology for potential applications as a natural treatment in chronic inflammation, neurodegenerative diseases, and skin improvement.

Extracellular vesicles (EVs) are membrane-bound particles of various sizes and compositions released by cells into the extracellular environment, serving as carriers of bioactive molecules such as proteins, lipids, and nucleic acids [6]. EVs are classified based on size, origin, and markers: exosomes (30–150 nm), which originate from the multivesicular bodies in the endosomal pathway; microvesicles (100–1000 nm), which bud directly from the plasma membrane; apoptotic bodies (1000-5000 nm), which are formed from membrane blebbing in apoptotic cells [6, 7]. These vesicles play essential roles in intercellular communication, modulating physiological and pathological processes by delivering molecular signals to recipient cells [6]. Due to their stability and biocompatibility, EVs have been explored for applications ranging from drug delivery and diagnostics to regenerative medicine, as well as skin therapies via non-invasive topical applications [7, 8].

Plant-derived EVs share similarities with mammalian EVs. For example, exosome-like particles in plants also form from multivesicular bodies akin to processes in mammalian cells [9]. Recently, plant-derived EVs have attracted considerable attention as an alternative to mammalian EVs due to their comparable therapeutic potential and additional advantages in safety, scalability, cost-effectiveness, and ethical sourcing [9, 10]. Plant-derived RNA, particularly microRNAs (miRNAs), can be found in EVs and play a significant role by influencing gene expression in recipient cells, particularly via cross-kingdom communication, where they can modulate the expression of target genes in other organisms, including humans [11]. Recent studies have shown that exosome-like EVs from plants, including *C. asiatica*, promote skin improvement and wound healing more effectively than conventional plant extracts [12]. For instance, *C. asiatica* exosome-like EVs can upregulate the COLA1 collagen gene and downregulate the MMP1 matrix metalloproteinase gene, and inhibit melanogenesis genes [13]. Furthermore, *C. asiatica* exosome-like EVs can be absorbed into human live cancer cell culture within 24 hours and exhibit anticancer effects by promoting apoptosis of cancerous cells [14].

Many medicinal plants, including *C. asiatica*, are subject to overharvesting, which threatens biodiversity and ecosystem health. By using tissue culture techniques, EVs can be obtained without

putting strain on ecological resources, supporting conservation efforts and ethical sourcing while meeting production demand [15]. In light of the therapeutic potential of *C. asiatica* and the unique properties of EVs as skin-penetrating biomolecular vehicles, this study aims to investigate the *in-vitro* properties of EVs isolated from *C. asiatica* tissue culture as well as the effects of *C. asiatica* EV-based gel on UV-induced skin damage in a mouse model.

Materials and Methods

Isolation and characterization of *Centella asiatica* extracellular vesicles

C. asiatica EVs were extracted and isolated by a multi-step filtration and centrifugation. Briefly, tissue culture *C. asiatica* was homogenized, coarsely filtered to remove large debris, and centrifuged. Pellets were collected and filtered through a 0.45 µm filter, extracted and finally filtered through a 0.45/0.22 µm membrane filter.

The size and morphology of the *C. asiatica* EVs were analyzed with nanoparticle tracking analysis (NTA) and transmission electron microscopy (TEM). The NTA was performed with ZetaView® system (Particle Metrix, Germany). A sample for TEM was prepared by dropping 10 µL of the specimen onto a copper grid, followed by rest for 2 minutes and blotted dry with filter paper. Ten µL of uranyl acetate was then applied to the grid and excess liquid was again dried with filter paper, and the process was again repeated. Afterward, the grid was air-dried and subjected to the TEM procedure.

Cell culture

The B16F10 cell line (mouse melanoma cells, ATCC CRL6475, BCRC60031) was obtained from the Bioresource Collection and Research Center (BCRC), Taiwan. The cells were maintained in Dulbecco's Modified Eagle Medium (DMEM) (Hyclone, Logan, UT) supplemented with 10% fetal bovine serum (FBS) and 1% antibiotics. Human keratinocyte line HaCaT (AddexBio T0020001) was grown in high-glucose DMEM supplemented with 10% FBS, 4 mM/L-glutamine, and 1% antibiotic-antimycotic solution. Human foreskin fibroblast line HS68 (BCRC 60038) was grown in high-glucose DMEM supplemented with 10% FBS, 4 mM/L-glutamine, and 1% antibiotic-antimycotic solution. Human keratinocytes line Detroit 551 (BCRC 60118) was grown in Minimum Essential Medium (MEM) supplemented with 10% FBS, 0.1 mM non-essential amino acids, and 1.0 mM sodium pyruvate. All cells were maintained at 37°C in a humidified atmosphere containing 5% CO_2.

Cell viability assay

The 3-(4,5-dimethylthiazol-2-yl)-2,5 diphenyltetrazolium bromide (MTT) method was performed for B16F10 cells. Briefly, the cells were exposed to various concentrations of *C. asiatica* EVs for 24 hours, and the MTT solution was then added to the wells. The insoluble derivative of MTT produced by intracellular dehydrogenase was solubilized with an ethanol-DMSO (1:1) mixture. The absorbance of the wells at 570 nm was read using a microplate reader. For HaCaT and Detroit 551 cells, 1/10 volume of alamarBlue® (resazurin) reagent was added directly after 24 hours of EV treatment and incubated for 4 hours at 37°C. The absorbance was then read at 570 nm with 600 nm as a reference. In both assays, cell viability was calculated as the ratio of absorbance of the treated cells to control.

115 Thiazoline-6-sulfonic acid (ABTS) free radical scavenging assay

116 The ABTS free radical assays were conducted as previously outlined [16]. A 7 mM stock solution
117 of ABTS was reacted with 2.45 mM potassium persulfate, and the mixture was left to stand in the dark
118 for at least 6 hours before use. The absorbance at 734 nm was measured immediately after mixing
119 various concentrations of *C. asiatica* EVs (4×10^6, 1×10^7, and 2×10^7 particles/mL) with 1 mL of ABTS
120 solution to detect changes within 10 minutes. Vitamin C (0.9 mg/mL) and BHA (0.9 mg/mL) were used
121 as positive controls.

122 Intracellular reactive oxygen species (ROS) assay

123 The intracellular ROS assay was performed using an established method [17]. B16F10 cells were
124 cultured in 24-well plates and treated with various concentrations of *C. asiatica* EVs (1×10^9, 2.5×10^9,
125 and 5×10^9 particles/mL), Trolox® (0.05 mg/mL, positive control), or none (negative control) for 24
126 hours. The cells were then incubated with 24 mM H_2O_2 for 30 minutes to induce oxidative stress. After
127 incubation, 2′, 7′-dichloro-fluorescein diacetate (DCFH-DA) was added to the cells and cultured for 30
128 minutes. After treatment, the cells were washed with PBS and trypsinized with trypsin/EDTA. The
129 fluorescence intensities of DCF were measured at an excitation wavelength of 504 nm and an emission
130 wavelength of 524 nm using a Fluoroskan Ascent fluorescent reader (Thermo Scientific, Vantaa,
131 Finland).

132 Total polyphenol content assay

133 Different concentrations of *C. asiatica* EVs (2×10^7, 4×10^7, 5×10^7 particles/mL) and gallic acid
134 standard were mixed with Folin-Ciocalteu reagent and incubated for 5 minutes. Sodium carbonate
135 solution was added and incubated for 30 minutes. The absorbance at 765 nm was measured using a
136 spectrophotometer and the gallic acid equivalent was calculated with the gallic acid standard curve
137 [18].

138 Metal chelating assay

139 The metal chelating activity of the extracellular vesicles was performed with potassium
140 ferricyanide ($K_3[Fe(CN)_6]$) assay [19]. Different concentrations of *C. asiatica* EVs (2×10^7, 5×10^7, 1×10^8
141 particles/mL) were mixed with 0.2 mM PBS and 1% (W/V) $K_3[Fe(CN)_6]$, with 2 mg/mL EDTA as the
142 positive control and deionized water as the blank control. The mixtures were heated at 50°C for 20
143 minutes. After cooling to room temperature, 10% (W/V) TCA was added, and the mixtures were
144 centrifuged at 12,000 rpm and 4°C for 5 minutes. The supernatants were transferred to a 96-well plate,
145 followed by the addition of deionized water and 1% (W/V) $FeCl_3$. The plates were incubated in the
146 dark for 30 minutes. Absorbance was measured at OD 700 nm to assess metal chelating activity.

147 Intracellular melanin content assay

148 The intracellular melanin content was measured as described previously [20]. B16F10 cells were
149 treated with α-Melanocyte-stimulating hormone (α-MSH, 100 nM) for 24 h to induce melanin
150 production. Following this, the cells were treated with different concentrations of *C. asiatica* EVs
151 (1×10^9, 2.5×10^9, and 5×10^9 particles/mL), or the positive control, arbutin (0.54 mg/mL), for an
152 additional 24 hours. Post-treatment, cell pellets containing a known number of cells were solubilized

153 in 1 N NaOH at 60°C for 60 minutes. The melanin content was then assayed at 405 nm.

154 Intracellular tyrosinase activity assay

155 The intracellular tyrosinase activity was determined as described in previous research [21].
156 B16F10 cells were treated with α-Melanocyte-stimulating hormone (α-MSH, 100 nM) for 24 hours to
157 induce melanin production. Following this, the cells were treated with different concentrations of *C.*
158 *asiatica* EVs (1×10^9, 2.5×10^9, and 5×10^9 particles/mL), or the positive control, arbutin (0.54 mg/mL),
159 for an additional 24 hours. After treatments, the cell extracts (100 μL) were mixed with freshly
160 prepared L-DOPA solution (0.1% in PBS) and incubated at 37°C. The absorbance at 490 nm was then
161 measured to assess the tyrosinase activity.

162 Type I procollagen (PIP) ELISA assay

163 Hs68 cells were seeded at 1×10^5 cells per well in 12 well plates and were cultured in 10% FBS
164 DMEM medium at 37°C with 5% CO_2 for 24 hours. After three washes with PBS, several different
165 concentrations ($1x10^7$, $1x10^8$, $1x10^9$) of *C. asiatica* EVs and 5 ng/mL TGF-β1 (AbCam Cat. #ab50036, as
166 positive control) were added and cultured for 24 hours. The level of type I procollagen in cell culture
167 supernatants was determined using a commercial PIP EIA Kit (TAKARA Cat. # MK101) according to the
168 manufacturer's instruction (2 step procedure).

169 mRNA expression of aquaporin-3 (AQP3) and filaggrin (FLG) genes

170 HaCat cells were dispensed into a 96-well plate and cultured for 24 hours under cell culture
171 conditions. Various concentrations of *C. asiatica* EVs and negative control (purified water only) were
172 added to the cells and cultured for 24 hours. Real-time PCR was performed to confirm the expression
173 of aquaporin-3 (AQP3) and filaggrin (FLG) at the gene level, and the test sequence is as follows. For
174 RNA isolation and cDNA synthesis, SuperPrep TM cell lysis & RT Kit for qPCR (TOYOBO, Cat. SCQ-101)
175 was used. To compare and analyze gene expression, the cDNA synthesized above was used as a
176 template, and Real-time PCR analysis was performed using Thunderbird TM SYBR qPCR Mix (TOYOBO,
177 Cat. QPS-201). The gene expression levels of the sample were quantified by normalization with
178 GAPDH using the $2^{-\triangle\triangle Ct}$ method.

179 mRNA expression of pro-inflammatory genes after UVB induction

180 HaCat cells ($1x10^4$/well for 96-well) or Hs68 cells ($5x10^4$/well for 24-well) were cultured for 24
181 hours and exposed to UVB at 90mJ dose. Various concentrations of *C. asiatica* EVs and negative
182 control (purified water only) were added to the cells and cultured for 4 hours. Real-time PCR was
183 performed to confirm the expression of cyclooxygenase-2 (COX) gene as above and the gene
184 expression levels were quantified by normalization with GAPDH using the $2^{-\triangle\triangle Ct}$ method.

185 Measurement of nitric oxide production

186 RAW 264.7 macrophage cells were seeded in 10% FBS DMEM medium in 24-well plates at a
187 density of 2×10^5 cells/well and were cultivated at 37°C with 5% CO_2 for 24 hours. Removing the
188 original medium, the cells were treated with $1x10^7$, $1x10^8$, $5x10^8$, $1x10^9$, $2x10^9$, or $4x10^9$ particles/mL
189 of *C. asiatica* EVs or gallic acid (10 and 20 μg/mL, Sigma-Aldrich Cat. #G7384) in serum-free DMEM
190 medium and incubated for 4 hours. After the pre-incubation, the cells were stimulated with 100

ng/mL LPS and incubated for 20 hours. The culture supernatants were harvested and centrifuged at 7,000 × g for 3 minutes. The samples were mixed with an equal volume (100 µL) of Griess reagent (Sigma-Aldrich Cat. #G4410) and the absorbance was measured at 540 nm after reacting for 10 minutes.

Animal study

Twelve male ICR mice were obtained from BioLASCO Taiwan Co. Ltd. (Taipei City, Taiwan). The mice were 7 weeks old and weighed from 31 to 33 g at the start of the study. The mice were randomly assigned to four groups with three mice in each of the group as in Table 1:

Table 1. Group assignment for the animal study.

Groups	Description	# of mice
UVB	UVB exposure only	3
Control	UVB exposure + gel without active ingredients	3
Treatment 1	UVB exposure + gel with purified *C. asiatica* EVs	3
Treatment 2	UVB exposure + gel with purified *C. asiatica* EVs + TECA (Titrated extract of *C. asiatica*)	3

To remove hair for test gel administration, mice were anesthetized with Isoflurane (3% – 4%), and back hair was shaved and further removed using hair removal cream. On Day 0, mice were exposed to 120 mJ/cm^2 UVB for 5 minutes to induce skin damage. From Day 0, after UVB exposure, the test gel was applied twice daily at a volume of 180–200 µL on the mice's back according to the respective group assignments. Photographs of the hair removal area were taken before UVB exposure on Day 0 and daily from Day 1 to Day 7 before applying the gel to observe skin repair. Body weight of the animals were measured on Days 0, 1, 4, and 7. Animals were sacrificed on Day 7 for histopathological analysis.

Animal tissue histopathological analysis

On the day of sacrifice, skin tissue samples were taken from back and fixed in 10% neutral formalin for at least 24 hours, embedded, and sectioned. The long axis of the skin tissue section was defined as the observation direction. After gradient alcohol dehydration, xylene permeation, and paraffin embedding, the skin tissue was cut into several continuous thin sections, each 4–6 µm thick. The first set of slides was stained with H&E, and five random fields were photographed at 200× magnification. Epidermal thickness was measured six times per field. The second set of sections was rehydrated, and antigen retrieval was performed using a pH 6 recovery solution. Immunohistochemistry (IHC) staining was conducted using rabbit anti-mouse myeloperoxidase antibody (Ab65871, Abcam Ltd, USA) at a concentration of 1 µg/mL, followed by goat anti-rabbit secondary antibody (GTX83399, GeneTEX, Taiwan) to stain antigen-positive cells in the dermis. Hematoxylin stain was then used as a counterstain. Six dermal areas were observed at 400×

magnification. Based on the presence of positive multinucleated cells, infiltrating cell counts were categorized into five grades according to ISO 10993-6 2016: Table E1 [26]: 0 points (negative); 1 (1–5 positive cells per field); 2 (6–10 positive cells per field); 3 (abundant infiltration of positive cells); 4 (field densely packed with positive cells).

Statistical analysis

Results are presented as the mean of the values, with error bars representing the 95% confidence intervals. The analysis package in GraphPad Prism 6.01 (Boston, MA) was used for statistical analysis. Statistical results were calculated by one-way ANOVA with Dunnett's multiple comparisons test.

For statistical analysis of tissue histopathology, Fisher's exact test was applied using the control group as the reference. A threshold of grade 3 or above was set for classification. The odds ratio (O.R.) was calculated using a one-tailed test. If the O.R. was less than 1, it indicated an effective treatment outcome; if greater than 1, the treatment was considered ineffective.

Ethical statements

All animal works were supervised by a licensed veterinarian and performed in a GLP-compliant animal testing facility. All animal studies were reviewed and approved by the Institutional Animal Care and Use Committee (IACUC) of a qualified institute in Taiwan. All procedures involving study animals were conducted in a manner that avoided or minimized discomfort, distress or pain to the animals. Clinical symptoms were observed once per day on behavior, respiration, and appearance.

Results

Isolation and characterization of *C. asiatica* EVs

C. asiatica EVs were isolated from tissue culture *C. asiatica* by a centrifugation and filtration. The size distribution of EVs harvested was analyzed by NTA and showed that the particle has a mean size of 150 nm (Figure 1A). The morphological features shown by the TEM images can be observed as vesicles of approximately 100-150 nm in size with a lipid bilayer membrane structure (Figure 1B).

Cytotoxicity assessment

To investigate the effect of *C. asiatica* EVs in cells, an MTT assay was used to evaluate the effect of cell viability. B16F10 melanoma cells were treated with various concentrations of *C. asiatica* EVs and MTT assay was performed. The results showed no significant differences compared to the control group in this test (Figure 2). Thus, high concentrations of up to 5×10^9 particles/mL of *C. asiatica* EVs do not exhibit cytotoxicity in B16F10 cells. In addition, no discernable differences in cell viability were detected in HaCaT and Detroit 551 cell lines, confirming that the EVs do not exhibit cytotoxicity in mouse or human cells (Figure S1).

Antioxidant activity assessment

A variety of naturally-occurring polyphenol compounds from *C. asiatica* extracts have0 been studied, which contribute to its antioxidant properties [5]. Here we investigated the total polyphenol content of *C. asiatica* EVs using an established method with the Folin-Ciocalteu reagent. The results showed that the gallic acid equivalent of *C. asiatica* EVs increased with the particle number, indicating

260 that the antioxidant activity of the vesicles may be dose-dependent (Figure S2).

261 We also assessed the antioxidant activity of *C. asiatica* EVs by using two cell-free assays: ABTS
262 and $K_3[Fe(CN)_6]$ assays. At the higher concentrations, *C. asiatica* EVs exhibited comparable $ABTS^{+\cdot}$
263 scavenging capacity to positive controls vitamin C and BHA (Figure S3). For the $K_3[Fe(CN)_6]$ metal
264 chelating assay, the results showed that reducing capacities of EVs were also dose-dependent (Figure
265 S4).

266 To further confirm the antioxidant capacity of *C. asiatica* EVs in B16F10 cells, intracellular
267 reactive oxygen species (ROS) levels were measured by ROS scavenging rate using H_2O_2 at 20 mM to
268 induce oxidative stress. After treatment, the intracellular ROS clearance was 53.86 ± 0.94%, 59.32 ±
269 1.68% and 66.27 ± 1.10% for $1x10^9$, $2.5x10^9$ and $5x10^9$ (particles/mL) of *C. asiatica* EVs, respectively
270 (Figure 3). The results showed that all concentrations of *C. asiatica* EVs significantly increased ROS
271 scavenging activity compared to the control group ($P<0.001$), demonstrating effects similar to positive
272 control Trolox.

273 Melanin inhibitory activity assessment

274 In addition to its antioxidant properties, *C. asiatica* has potential for skin whitening application
275 through the inhibition of melanin synthesis [22]. First, we investigated its inhibition of melanin
276 production in B16F10 melanoma cells treated with α-melanocyte-stimulating hormone (α-MSH). After
277 *C. asiatica* EV treatment, the melanin content in the B16F10 cells was 93.55 ± 1.14%, 90.73 ± 1.17%
278 and 83.69 ± 4.31% of control at $1×10^9$, $2.5×10^9$ and $5×10^9$ particles/mL of *C. asiatica* EVs, respectively
279 (Figure 4A). For the positive standard arbutin (0.54 mg/mL), the remaining intracellular melanin
280 content was 71.95 ± 2.44% of the control. Tyrosinase catalyzes the first two steps of melanin synthesis
281 by hydroxylation of L-tyrosine to L-DOPA [23]. Therefore, to investigate the change in melanin
282 synthesis via tyrosinase activity, we have carried out intracellular tyrosinase activity in B16F10 cells
283 treated with α-MSH. After treatment, the remaining intracellular tyrosinase activity was 92.5 ±
284 6.77%, 80.2.7 ± 5.13% and 56 ± 3.83% for the $1x10^9$, $2.5x10^9$ and $5x10^9$ particles/mL of either *C.*
285 *asiatica* EVs, respectively (Figure 4B). In comparison, the remaining intracellular tyrosinase activity
286 was 66 ± 10.53% of control after the cells were treated with arbutin, a known skin-whitening
287 compound. The results indicated that $5x10^8$ particles/mL of *C. asiatica* EVs exhibited stronger
288 inhibitory effect on α-MSH induced tyrosinase activity in B16F10 cells than arbutin, albeit with higher
289 intracellular melanin content than arbutin.

290 Effect of *C. asiatica* on skin integrity-related genes

291 One of the major components in skin tissue is type I collagen, which is derived from its precursor
292 type I procollagen (PIP) secreted by skin fibroblasts, and lowered expression of PIP is associated with
293 skin UV damage and senescence leading to wrinkle formation [24]. *C. asiatica* EVs increased
294 production of PIP in Hs68 cells and induced a similar expression level of PIP to that of positive control
295 TGF-β1 at the highest concentration tested ($1x10^9$ particles/mL) (Figure S5). Aquaporin and filaggrin
296 are important in the barrier function of skin by regulating water transport and water retention in skin
297 [25]. Real-time PCR assay quantification of mRNA expression of aquaporin-3 (AQP3) and filaggrin (FLG)

genes in HaCaT keratinocyte cells treated with *C. asiatica* EVs showed that *C. asiatica* EVs could upregulate the expression levels of AQP3 and FLG genes compared to the control group (Figure S6).

Anti-inflammatory effects of *C. asiatica* EVs

UV exposure of keratinocyte can induce COX2 expression that increases pro-inflammatory prostalglandin synthesis, and *C. asiatica* triterpene madecassoside was found to inhibit UV-induced inflammation [22]. Here we showed that addition of *C. asiatica* EVs can lower expression levels of COX2 in skin fibroblast Hs68 and keratinocyte HaCaT cells exposed to UV (Figure S7). Nitric oxide (NO) is an inflammatory response messenger secreted mainly by endothelial cells and macrophages, as well as keratinocytes, and exposure of skin to UV irradiation results in elevated levels of NO production [27]. We subjected *C. asiatica* EV-treated RAW 264.7 macrophage culture to lipopolysaccharide (LPS), which is a TLR4 ligand and induces pro-inflammatory response [28]. The NO production was measured by Griess reagent, which is converted to a pink color after reacting with nitrites. As shown in Figure 5, the amount of nitrite decreases in a dose-dependent manner in cells treated with increasing concentrations of EVs. Taken together, *C. asiatica* EVs were able to reduce UV-induced inflammatory response in a variety of cell types tested.

Effect of *C. asiatica* EV-based gel on UVB-induced skin damage in Mice

Next, we investigated whether a *C. asiatica* EV-based gel formulation (with or without addition of *C. asiatica* extract TECA) could alleviate skin damage induced by UVB exposure. First, we evaluated the safety of the application of *C. asiatica* EV gel and we found no adverse effects in all groups that were applied with gel, regardless of the presence of *C. asiatica* EV or TECA (Table S1). There were also no significant weight differences between groups ($p > 0.05$), despite a slight decrease in body weight during the study in all groups (Table S2 and Figure S8).

In tissue histopathological analysis, the epidermis measurement results are summarized in Table 2 and Figure 6. The UVB-only group had slightly less epidermis thickness (126.66 ± 47.73 μm) compared to the control group (154.94 ± 58.14 μm), but the difference was not statistically significant. Treatment groups 1 and 2 had average epidermal thicknesses of 87.66 ± 35.32 μm and 86.09 ± 25.74 μm, respectively. Compared to the control group (154.94 ± 58.14 μm), the epidermal thicknesses were significantly ($p < 0.01$ for treatment 1 and $p < 0.05$ for treatment 2) reduced.

In addition, immunohistochemical staining of inflammation marker myeloperoxidase (MPO) was used to observe positive multinucleated cells in the dermis of UV-damaged areas (Table 2 and Figure 7). In both UVB-only and control groups, 75% of the observed fields exhibited extensive infiltration of positive multinucleated cells. The addition of *C. asiatica* EVs with or without TECA significantly reduced cellular infiltration (8.3% in both treatment groups). The odds ratios were also significantly lower in both treatment groups (0.03) compared to UVB and control groups (1.00) as calculated by Fisher's exact test.

Table 2 Tissue section measurement and observation. Results are taken from measurements of two skin sections (5 random fields for H&E stain, 6 random fields for IHC stain)

	UVB	Control	Treatment 1	Treatment 2
	H&E stain-epidermis thickness (mean ± SD in µm) (N = 10 random fields)			
Results	126.66 ±47.73[NS]	154.94 ±58.14	87.66 ±35.32[*]	86.09 ±25.74[**]
	IHC stain-Number of positives/Total number observed (N = 12 random fields)			
Myeloperoxidase-positive (score ≥3)	9/12[NS]	9/12	1/12[**]	1/12[**]
Odds ratio (95% CI)	1.00	1.00	0.03	0.03

[NS]: Statistically not significant compared to control group

[*]: Statistically significant compared to control group ($p < 0.01$).

[**]: Statistically significant compared to control group ($p < 0.05$).

Gross appearance examination of mouse skin UVB exposure site on Day 6 of the study is shown in representative photographs in Figure 8. In UVB-only and blank gel control groups, inflammation and redness are still apparent at the UV wound site, with only a few newly repaired skin and abundant scarring. In contrast, for both treatment groups, the wound has been repaired and inflammation is absent at the site with minimal scarring.

Discussion

In this study, we have isolated and characterized EVs secreted from *C. asiatica* tissue culture. The EVs have a size of approximately 150 nm and a lipid bilayer morphology similar to that previously reported for exosomes derived from *C. asiatica* and other plants [12, 13]. In a series of *in-vitro* experiments in B16F10 cell culture, we have demonstrated that the EVs are safe for cells and that EVs exhibited notable antioxidant, anti-melanogenic, and anti-inflammatory effects, suggesting potential applications in skin care and therapeutic treatments to combat oxidative stress and hyperpigmentation. Another study also isolated exosome-like EVs from *C. asiatica* but with a smaller average particle size of 63.8 nm [14]. While the EVs from the above study exhibited cytotoxicity in HepG2 human cancer cells, we did not observe any effect on cell viability in mouse melanoma B16F10 cells or HaCaT and Detroit 551 human cell lines tested (Figures 2 and S1) [14]. The therapeutic properties of *C. asiatica* have mostly been attributed to the triterpenes and derivatives, including madecassoside, madecassic acid, asiaticoside, and asiatic acid, and these are among the most well-studied compounds in the plant [3-5]. In our study, we observed potent antioxidant effects from *C. asiatica*, although further study is required to determine specifically how contents within EVs (chemicals, proteins, and nucleic acids) can contribute to observed effects. In addition to phytochemicals and proteins, small RNAs and miRNAs in EVs are important modulators of target effect proteins, and RNA binding proteins, such as Argonaute 1, RNA helicases, and Annexins, may be involved in packing RNA into EVs [10, 28] A recent preprint study has provided a comprehensive analysis of the transcriptome human skin keratinocytes after treatment of *C. asiatica* exosomes, revealing 11 novel miRNAs packed within the exosomes [13]. The above study also found that skin integrity and barrier-related genes were upregulated after treatment by *C. asiatica* EVs, which we have also observed in this study with increasing gene expression of PIP1, AQP3, and FLG (Figures S5

369 and S6) [13]. The study also found that *C. asiatica* exosomes induced higher gene expression than *C.*
370 *asiatica* extracts, possibly due to better penetration of skin cells by exosomes and the presence of
371 miRNAs [13]. Thus *C. asiatica* EVs could provide their effect via multitude of effectors such as
372 phytochemicals and miRNAs.

373 In *C. asiatica,* madecassoside by itself has the ability to inhibit UV-induced melanin synthesis in a
374 keratinocyte and melanocyte co-culture system as well as artificially tanned human skin [22]. Other
375 plant-derived EVs also have anti-melanogenic effect. For example, *Dendropanax morbifera* EVs can
376 inhibit the expression of melanogenesis genes such as MITF, TYR, TRP-1, and TRP-2 [9, 28]. In our
377 study, the EVs appeared to modulate melanogenesis pathways in cell culture, likely through the
378 inhibition of tyrosinase activity, which is a key enzyme in melanin synthesis [23]. The mechanism of
379 anti-melanogenesis by *C. asiatica* includes inhibition of inflammation, as observed in previous studies
380 [24]. and in our study, where we have observed that *C. asiatica* can reduce pro-inflammatory gene
381 expression, such as COX2 and decrease the production of NO (Figures 5 and S7). As melanin
382 overproduction contributes to skin conditions like freckles and nevus formation, and age spot
383 development, plant-derived EVs with anti-melanogenic properties represent an economical and
384 natural alternative to conventional treatments, which often come with side effects or limited efficacy
385 [29].

386 In the animal study, mice were exposed to UVB at 120 mJ/cm^2 for 5 minutes to induce
387 photoaging and skin damage. This was followed by daily application of EV gel for seven consecutive
388 days. Photoaging leads to degeneration of elastic fibers and collagen loss, resulting in epidermal
389 thickening of the stratum corneum [30]. In both treatment groups consist of *C. asiatica* EV gels with or
390 without TECA, we observed reduced epidermal thickening in skin sections and reduced cell infiltration
391 due to inflammation characterized using IHC staining, suggesting a potential skin repair effect.
392 However, in the control group with blank gel application, thicker, albeit not statistically significant,
393 epidermis layer was observed than UVB-only group, possibly due to mechanical irritation from the gel
394 application process. These preliminary results suggest that EVs may help to alleviate UV-induced
395 inflammation but are unable to reverse UV-induced epidermal damage.

396 The tissue culture micropropagation technology for *C. asiatica* has been established as a
397 sustainable source of *C. asiatica* [31]. This ensures its conservation in nature while providing a
398 constant yield of raw material, akin to the use of bioreactors in biopharmaceutical drug and vaccine
399 production. Using plant tissue culture as a source for EV production presents several advantages over
400 traditional methods of harvesting from wild plants. First, tissue culture allows for consistent, scalable
401 production of EVs with genetic uniformity, bypassing the variability associated with environmental
402 factors that affect wild plants, such as seasonal changes, soil quality, and climate/geographical
403 conditions [15, 29]. This standardization is particularly important for achieving reproducible results in
404 therapeutic and cosmetic applications, where consistent quality and efficacy are crucial in ensuring
405 the safety and efficacy of the product. Additionally, tissue culture can be optimized to enhance the
406 yield of specific bioactive compounds through controlled environmental conditions and the use of

elicitors [15].

In conclusion, this *in vitro* and animal model study demonstrated the antioxidant, anti-melanogenic and anti-inflammatory potential of *C. asiatica*-derived EVs from tissue culture. The advantages of tissue culture over wild plants in terms of sustainability, consistency, and the ability to enhance bioactive compound production further support the use of this approach in developing plant-based EV therapies. Future studies could focus on characterizing bioactive molecules and miRNAs within these EVs, as well as exploring their safety and efficacy in *in-vivo* models. Ultimately, this work paves the way for the sustainable production and utilization of plant-derived EVs in skin care cosmetics and wound healing applications.

Acknowledgements

We thank the team of Schweitzer Biotech Company for reading and providing feedback for preparation of the manuscript.

Competing Interests

C.-C. W., C.-H. C., P.-L. K., W.-H. T., L. T.-C. L., C. C., and T.-Y. K. are employees of Schweitzer Biotech Company. W.-Y. Q. and I. P. are consultants employed by Schweitzer Biotech Company. T.-M. C. and S.-S. W. have no competing interests to declare. This study is funded by Schweitzer Biotech Company.

References

1. Biswas D, Mandal S, Chatterjee Saha S, Tudu CK, Nandy S, Batiha GE, Shekhawat MS, Pandey DK, Dey A (2021) Ethnobotany, phytochemistry, pharmacology, and toxicity of Centella asiatica (L.) Urban: A comprehensive review. Phytother Res 35:6624–6654. https://doi.org/10.1002/ptr.7248
2. Sabaragamuwa R, Perera CO, Fedrizzi B (2018) Centella asiatica (Gotu kola) as a neuroprotectant and its potential role in healthy ageing. Trends Food Sci Technol 79:88-97. https://doi.org/10.1016/j.tifs.2018.07.024
3. Bandopadhyay S, Mandal S, Ghorai M, Jha NK, Kumar M, Radha, Ghosh A, Proćków J, Perez de la Lastra JM, Dey A (2023) Therapeutic properties and pharmacological activities of asiaticoside and madecassoside: A review. J Cell Mol Med 27(5):593-608. https://doi.org/10.1111/jcmm.17635
4. Sun B, Wu L, Wu Y, Zhang C, Qin L, Hayashi M, Kudo M, Gao M, Liu T (2020) Therapeutic potential of Centella asiatica and its triterpenes: a review. Front Pharmacol 11:568032. https://doi.org/10.3389/fphar.2020.568032
5. Diniz LR, Calado LL, Duarte AB, de Sousa DP (2023) Centella asiatica and its metabolite asiatic acid: wound healing effects and therapeutic potential. Metabolites 13(2):276. https://doi.org/10.3390/metabo13020276

445 6. Jeppesen DK, Zhang Q, Franklin JL, Coffey RJ (2023) Extracellular vesicles and nanoparticles:
446 emerging complexities. Trends Cell Biol 33(8):667-81.
447 https://doi.org/10.1016/j.tcb.2023.01.002
448 7. Moghassemi S, Dadashzadeh A, Sousa MJ, Vlieghe H, Yang J, León-Félix CM, Amorim CA (2024)
449 Extracellular vesicles in nanomedicine and regenerative medicine: A review over the last
450 decade. Bioact Mater 36:126-56. https://doi.org/10.1016/j.bioactmat.2024.02.021
451 8. Yang GH, Lee YB, Kang D, Choi E, Nam Y, Lee KH, You HJ, Kang HJ, An SH, Jeon H (2021)
452 Overcome the barriers of the skin: exosome therapy. Biomater Res 25(1):22.
453 https://doi.org/10.1186/s40824-021-00224-8
454 9. Li A, Li D, Gu Y, Liu R, Tang X, Zhao Y, Qi F, Wei J, Liu J (2023) Plant-derived nanovesicles: Further
455 exploration of biomedical function and application potential. Acta Pharm Sin B 13(8):3300-20.
456 https://doi.org/10.1016/j.apsb.2022.12.022
457 10. Zhu Y, Zhao J, Ding H, Qiu M, Xue L, Ge D, Wen G, Ren H, Li P, Wang J (2024) Applications of
458 plant-derived extracellular vesicles in medicine. MedComm. 2024 5(10):e741.
459 https://doi.org/10.1002/mco2.741
460 11. Urzì O, Gasparro R, Ganji NR, Alessandro R, Raimondo S (2022) Plant-RNA in extracellular
461 vesicles: the secret of cross-kingdom communication. Membranes 12(4):352.
462 https://doi.org/10.3390/membranes12040352
463 12. Cho JH, Hong YD, Kim D, Park SJ, Kim JS, Kim HM, Yoon EJ, Cho JS (2022) Confirmation of
464 plant-derived exosomes as bioactive substances for skin application through comparative
465 analysis of keratinocyte transcriptome. Appl Bio Chem 65(1):8.
466 https://doi.org/10.1186/s13765-022-00676-z
467 13. Kim MH, Yoon EJ, Kim JS, Park SJ, Lee H (2023) Comparative analysis of the transcriptome and
468 efficacy of bioactive Centella asiatica exosomes on skin cells. ResearchSquare
469 https://doi.org/10.21203/rs.3.rs-2787704/v1
470 14. Huang J, Cao X, Wu W, Han L, Wang F (2024) Investigating the proliferative inhibition of HepG2
471 cells by exosome-like nanovesicles derived from Centella asiatica extract through
472 metabolomics. Biomed Pharmacother 176:116855.
473 https://doi.org/10.1016/j.biopha.2024.116855
474 15. Kumari S, Kumar N, Trivedi MP (2022) Application of Plant Tissue Culture for Improvement of
475 Centella asiatica. In: Kumar N (ed) Biotechnology and Crop Improvement, 1st ed. CRC Press,
476 Boca Raton, FL, pp. 93-106. https://doi.org/10.1201/9781003239
477 16. Re R, Pellegrini N, Proteggente A, Pannala A, Yang M, Rice-Evans C (1999) Antioxidant activity
478 applying an improved ABTS radical cation decolorization assay. Free Radic Biol Med
479 26(9-10):1231-7. https://doi.org/10.1016/S0891-5849(98)00315-3
480 17. Murrant CL, Reid MB (2001) Detection of reactive oxygen and reactive nitrogen species in
481 skeletal muscle. Microsc Res Tech 55(4):236-48. https://doi.org/10.1002/jemt.1173
482 18. Singleton VL, Orthofer R, Lamuela-Raventós RM (1999) Analysis of total phenols and other

483 oxidation substrates and antioxidants by means of folin-ciocalteu reagent. In: Packer L (ed)
484 Methods in enzymology. Academic Press, Cambridge MA, Vol. 299, pp. 152-178.
485 https://doi.org/10.1016/S0076-6879(99)99017-1
486 19. Adjimani JP, Asare P. (2015) Antioxidant and free radical scavenging activity of iron chelators.
487 Tox Rep 2:721-8. https://doi.org/10.1016/j.toxrep.2015.04.005
488 20. Tsuboi T, Kondoh H, Hiratsuka J, Mishima Y (1998) Enhanced melanogenesis induced by
489 tyrosinase gene-transfer increases boron-uptake and killing effect of boron neutron capture
490 therapy for amelanotic melanoma. Pigment Cell Res 11(5):275-82.
491 https://doi.org/10.1111/j.1600-0749.1998.tb00736.x
492 21. Yang JY, Koo JH, Song YG, Kwon KB, Lee JH, Sohn HS, Park BH, Jhee EC, Park JW (2006)
493 Stimulation of melanogenesis by scoparone in B16 melanoma cells 1. Acta Pharmacol Sin
494 27(11):1467-73. https://doi.org/10.1111/j.1745-7254.2006.00435.x
495 22. Jung E, Lee JA, Shin S, Roh KB, Kim JH, Park D (2013) Madecassoside inhibits melanin synthesis
496 by blocking ultraviolet-induced inflammation. Molecules 18(12):15724-36.
497 https://doi.org/10.3390/molecules181215724
498 23. Snyman M, Walsdorf RE, Wix SN, Gill JG (2024) The metabolism of melanin synthesis—From
499 melanocytes to melanoma. Pigment Cell Melanoma Res 37(4):438-452.
500 https://doi.org/10.1111/pcmr.13165
501 24. Talwar HS, Griffiths CE, Fisher GJ, Hamilton TA, Voorhees JJ (1995) Reduced type I and type III
502 procollagens in photodamaged adult human skin. J Invest Dermatol 105(2):285-90.
503 doi: 10.1111/1523-1747.ep12318471
504 25. Park CH, Min SY, Yu HW, Kim K, Kim S, Lee HJ, Kim JH, Park YJ (2020) Effects of apigenin on
505 RBL-2H3, RAW264. 7, and HaCaT cells: anti-allergic, anti-inflammatory, and skin-protective
506 activities. Int J Mol Sci 21(13):4620. https://doi.org/10.3390/ijms21134620
507 26. International Organization for Standardization. (2016) ISO 10993-6:2016(En). Biological
508 Evaluation of Medical Devices — Part 6: Tests for Local Effects after Implantation. Geneva: ISO
509 27. Cals-Grierson MM, Ormerod AD (2004) Nitric oxide function in the skin. Nitric oxide
510 10(4):179-93. https://doi.org/10.1016/j.niox.2004.04.005
511 28. Mantovani A, Garlanda C (2023) Humoral innate immunity and acute-phase proteins. N Engl J
512 Med 388(5):439-52. https://doi.org/10.1056/NEJMra220634
513 29. Lee R, Ko HJ, Kim K, Sohn Y, Min SY, Kim JA, Na D, Yeon JH (2020) Anti-melanogenic effects of
514 extracellular vesicles derived from plant leaves and stems in mouse melanoma cells and
515 human healthy skin. J Extracell Vesicles 9(1):1703480.
516 https://doi.org/10.1080/20013078.2019.1703480
517 30. Liu H, Dong J, Du R, Gao Y, Zhao P. (2024) Collagen study advances for photoaging skin.
518 Photodermatol Photoimmunol Photomed 40:e12931. https://doi:10.1111/phpp.12931
519 31. Mohapatra P, Ray A, Sandeep IS, Nayak S, Mohanty S (2021) Tissue-Culture-Mediated
520 Biotechnological Intervention in Centella asiatica: A Potential Antidiabetic Plant. In: Gantait S,

521 Verma SK, Sharangi AB (eds) Biotechnology of Anti-diabetic Medicinal Plants. Spring, Singapore,
522 pp. 89-116. https://doi.org/10.1007/978-981-16-3529-8_4
523 32. Park JH, Choi JY, Son DJ, Park EK, Song MJ, Hellström M, Hong JT. (2017) Anti-inflammatory
524 effect of titrated extract of Centella asiatica in phthalic anhydride-induced allergic dermatitis
525 animal model. Int J Mol Sci 18(4):738. https://doi.org/10.3390/ijms18040738
526

Figures

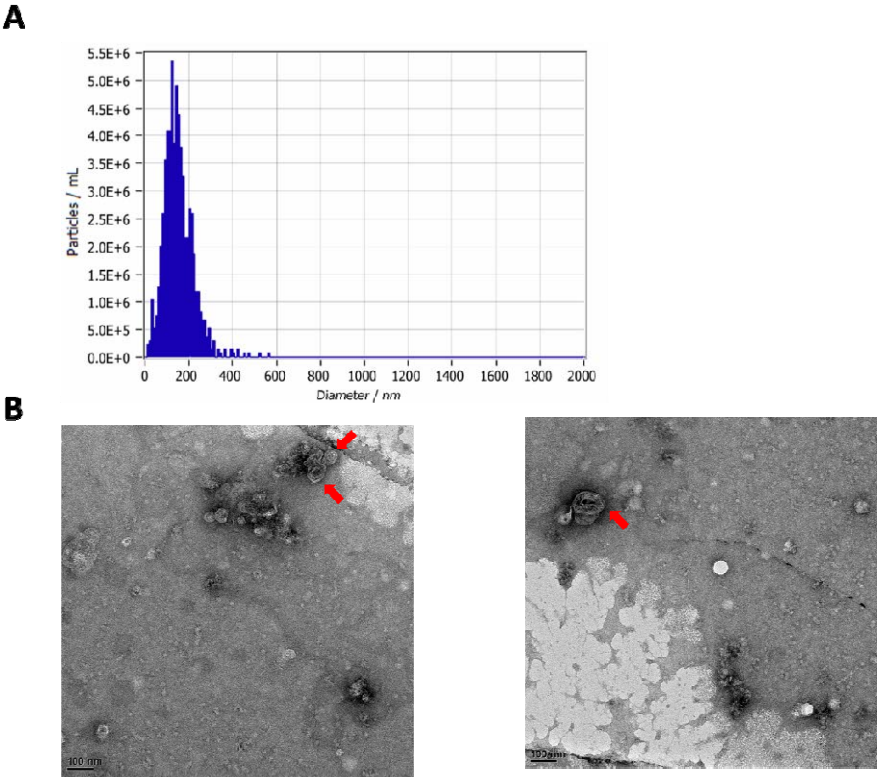

Fig. 1 Size and morphology characterization of *C. asiatica*-derived EVs. A. Nanoparticle tracking analysis (NTA) of size and concentration distribution of EVs by using the ZetaView® system. B. Representative TEM images of purified *C. asiatica* EVs with red arrows showing vesicles with lipid bilayer membrane structure. Scale bar: 100 nm

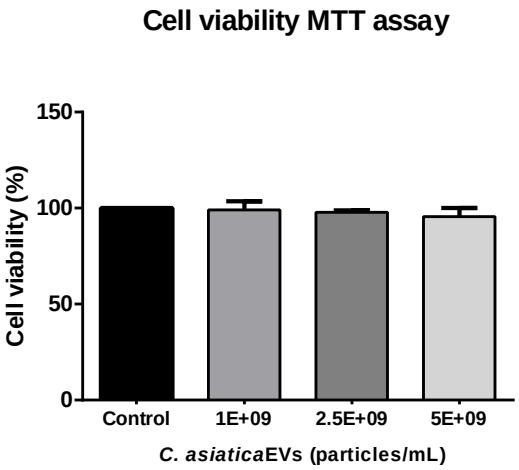

Fig. 2 Cell viability assay. B16F10 cells were treated with different concentrations of *C. asiatica* EVs. After 24h treatment, cell viability was measured by the MTT assay method. Data are presented as mean ± SD (n=3). Statistical results were calculated by one-way ANOVA with Dunnett's multiple comparisons test compared to the control group.

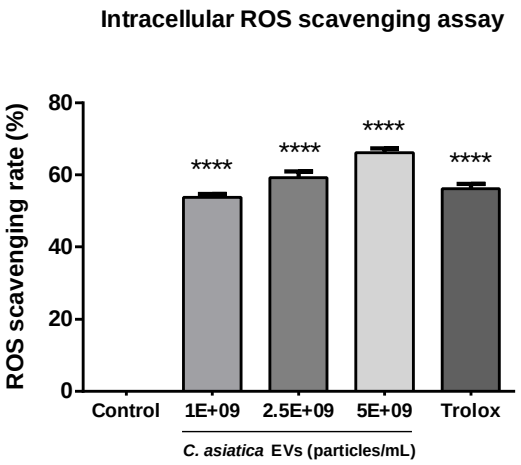

Fig. 3 Intracellular ROS level. B16F10 cells were pretreated with various concentrations of *C. asiatica* EVs, Trolox (0.05 mg/mL, positive control), or left untreated as a control for 24 hours. The cells were then incubated with 24 mM H_2O_2 and DCFH-DA. The fluorescence intensities of DCF were measured to calculate the ROS levels. Data are presented as mean ± SD (n=3). Statistical analysis was calculated by one-way ANOVA with Dunnett's multiple comparisons test, compared to the control group. ****P<0.0001

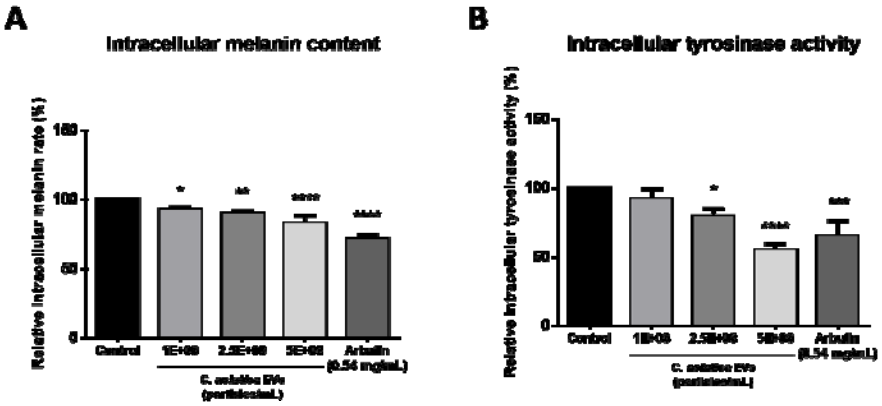

Fig. 4 Effect of *C. asiatica* EVs on melanin production. Inhibitory effects of different concentrations of *C. asiatica* EVs on **A.** melanin content and **B.** intracellular tyrosinase activity in B16F10 cells. Data are presented as mean ± SD (n=3). Statistical results were calculated by one-way ANOVA with Dunnett's multiple comparisons test compared to the control group. *P<0.05, **P<0.01, ***P<0.001, ****P<0.0001

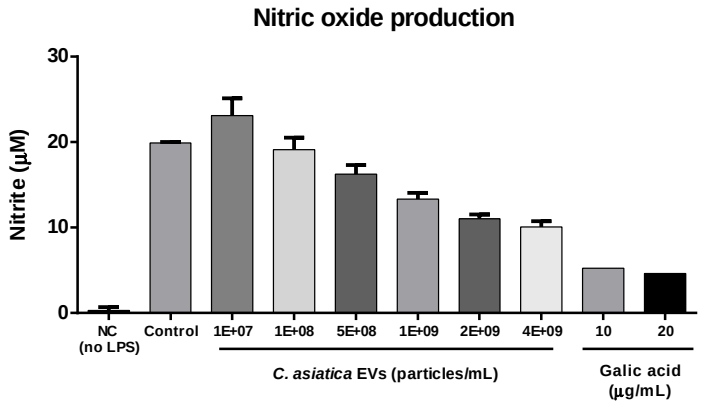

Fig. 5 Nitric oxide (NO) production in RAW 264.7 macrophages. Cells were treated with different concentrations of *C. asiatica* EVs or gallic acid after induction by LPS. The resulting NO produced was detected by the Griess reagent.

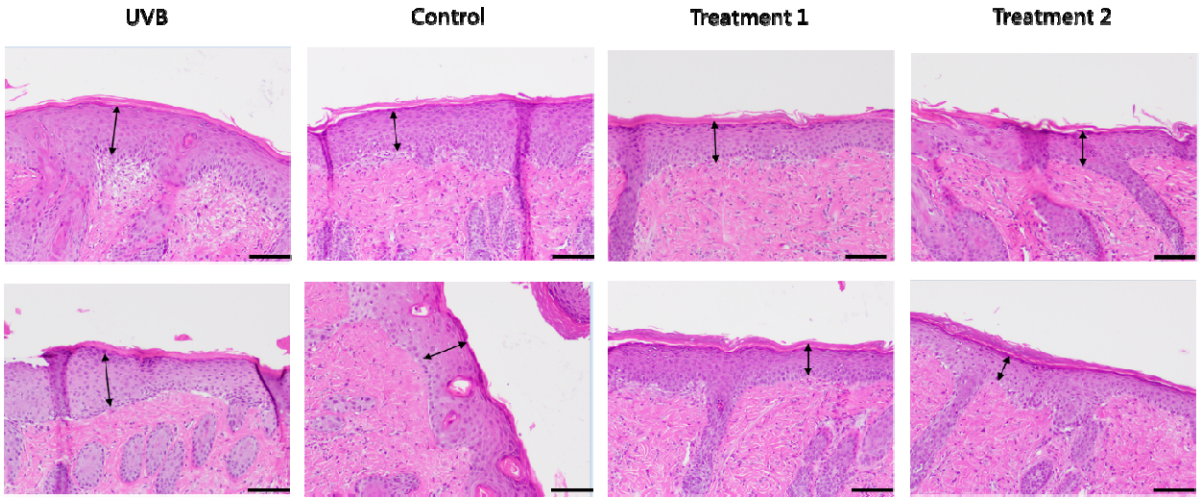

Fig. 6 Representative examples of histopathological analysis of skin tissue sections on Day 7 of the study. Arrows indicate thickness of the epidermis. H&E stain, 200x magnification (scale bar = 100 µm)

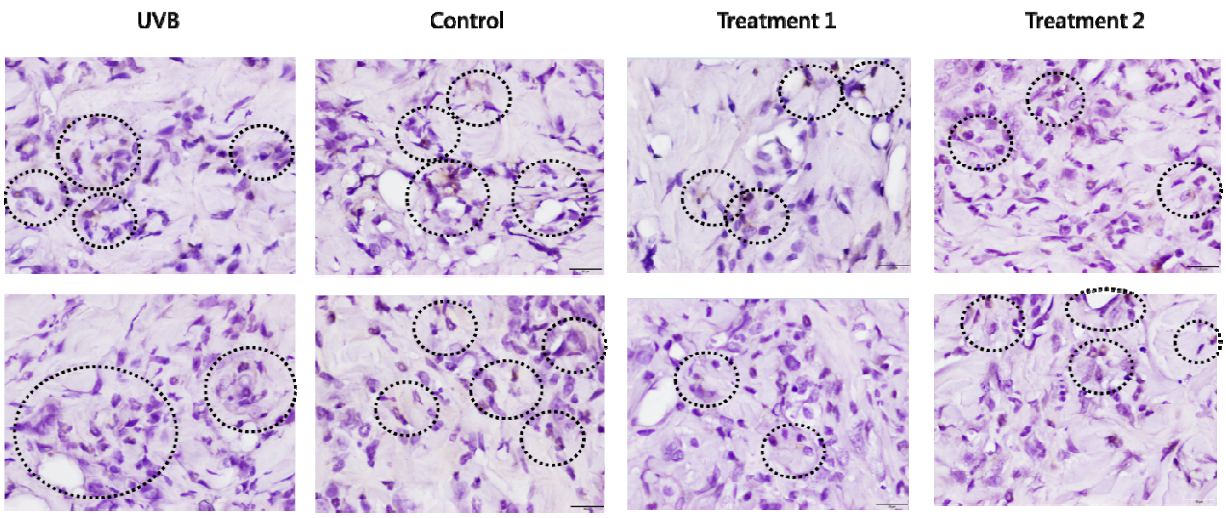

Fig. 7 Representative examples of IHC staining of myeloperoxidase (in brown, indicated by circles) in skin tissue sections on Day 7 of the study. Mouse back skin sections were stained with rabbit anti-mouse myeloperoxidase antibody and then detected by HRP goat anti-rabbit antibody. 400x magnification (scale bar = 20 µm)

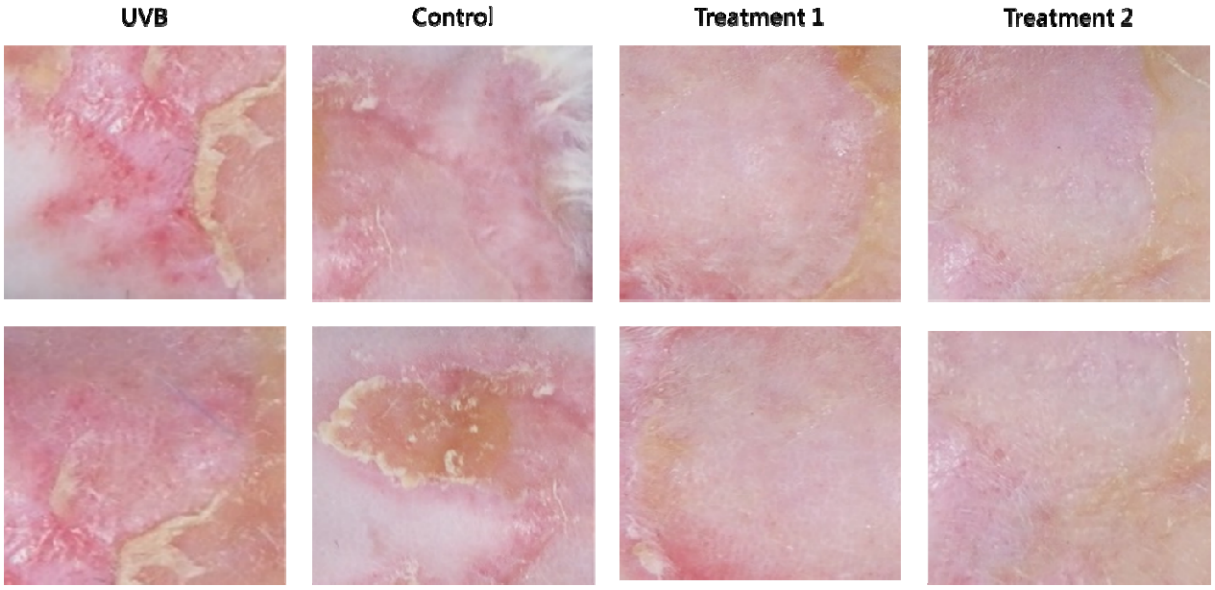

Fig. 8 Representative examples of mouse skin appearance at the site of UVB exposure on Day 6 of the study.